Journal of Photochemistry and Photobiology A: Chemistry 284 (2014) 36–48

Contents lists available at ScienceDirect

Journal of Photochemistry and Photobiology A: Chemistry

journal homepage: www.elsevier.com/locate/jphotochem

Tunable single and dual emission behavior of imidazole fluorophores based on D-π-A architecture

N. Nagarajan, G. Velmurugan, P. Venuvanalingam*, R. Renganathan*

School of Chemistry, Bharathidasan University, Tiruchirappalli 620024, Tamil Nadu, India

ARTICLE INFO

Article history:
Received 17 December 2013
Received in revised form 3 April 2014
Accepted 10 April 2014
Available online 21 April 2014

Keywords:
Imidazole
Dual emission
ICT
D-π-A
DFT/TDDFT

ABSTRACT

A series of three D-π-A molecules containing 4,5-diphenyl-1H-imidazole moiety as the donor (D) with cyanoacetic acid, rhodanine-3-acetic acid and 4-nitrophenyl acetonitrile as the acceptor (A) connected by a biphenyl bridge have been synthesized and characterized. Crystallography of BIC shows C4-phenyl group to be twisted nearly perpendicular to the imidazole unit and the remaining groups are in plane. The absorption spectra of the compounds are dominated by intramolecular charge transitions that arise from the imidazole core to the acceptor groups. The compounds display distinct dual and single emission behavior in different solvent environments, namely locally excited (LE ~ 430 nm) and intramolecular charge transfer (ICT ~ 550 nm). The Lippert–Mataga analysis suggested that the excited state dipole moment of ICT band is higher than the LE band. The influence of general and specific solvent effects on photophysical properties of the fluorophores was discussed with Catalán four parameter and Kamlet–Taft three parameter solvent scales. These results suggest that the major influence from solvent dipolarity takes part in a prominent role on changing the emission behavior of the compounds. The quantum yield of the compounds ranged between 0.07 and 0.55 in different solvents and it was shown to depend on the substitution pattern most notably that based on acceptor groups. All the compounds exhibit two lifetimes in the singlet excited state corresponding to LE state (short lived) and ICT state (long lived). In addition, the triplet state absorption properties of the compounds are also investigated by transient absorption measurement. The geometric structure and electronic structure of the molecules in the ground state is studied with DFT methods, whereas the energies of the lowest singlet excited states are calculated by employing TD-DFT methods. The results show that most prominent bands in acetonitrile solvent with higher oscillator strength for BIC, BIN and BIR are due to LE.

1. Introduction

A great deal of research efforts have been devoted on organic molecules featuring intramolecular charge transfer (ICT) in both photochemistry and biochemistry because of their notable applications in the field of sensors [1–3], molecular electronics, non-linear optics [4], dye sensitized solar cells [5,6] and pharmacology [7,8]. The electronic coupling between the locally excited (LE) state and the charge transfer (CT) state results in excited-state electron transfer in organic donor–acceptor compounds which in turn leads to the increased dipole moment in excited state, large Stokes shift and pronounced solvatochromic effect [9]. Organic π-conjugated molecules possessing electron donor and acceptor groups exhibiting the phenomenon of dual fluorescence are of special interest because of the potential tuning of the material properties by forming highly polar excited states and large charge separation [10] that can be manipulated using external stimuli. Several models have been studied to explain dual emission bands [11,12] observed in some electron donor–acceptor compounds. The energy dissipation of electronically excited state is mainly governed by hydrogen bonding and solvent polarity [13]. Considerable attention has been paid toward synthesis of diverse classes of donor–acceptor type fluorescent materials, which possess brilliant photophysical behavior, some typical examples being squarins [14], BODIPY [15], oligophenylenevinylenes [16], fluorescein [17], cyanine [18], rhodamine [19], pyridine [20], etc.

Imidazole, a biologically active compound, is well known in the medicinal field [21–24] as a drug with anticancer, antimicrobial, antibacterial, antifungal activities and as an antioxidant. In recent years, researchers have been employing imidazole compounds in optoelectronic (DSSC [25,26], OLEDs [27–29] and NLO [30]) applications because of its attractive properties. For instance,

* Corresponding authors. Tel.: +91 431 2407053; fax: +91 431 2407045.
E-mail address: rrengas@gmail.com (R. Renganathan).

http://dx.doi.org/10.1016/j.jphotochem.2014.04.008
1010-6030/

it can function both as an electron donor and acceptor. Moreover the rigidity of imidazole may help to reduce the reorganization energy during charge transfer and introduction of an auxiliary electron donor at positions 4 and 5, and its conjugation as well as electron acceptors at position 2 of imidazole favors the formation of conjugated dipolar compounds. Through appropriate modification of the conjugated chain, it is possible to tune the charge-transfer transition of dipolar molecules [31]. Continuous efforts have been put forward to enhance the performance of optoelectronic device by using various acceptor groups, *viz*., carboxylic acid [32,33], cyanoacetic acid [34,35], rhodanine-3 acetic acid [35], 4-nitrophenyl acetonitrile [36]. However, despite this effort, the influence of these different acceptor groups on its photophysical properties is not yet completely understood. Presumably, these groups are very sensitive to the solvent environments which drastically changes its absorption and emission behavior. In view of this, we synthesized 4,5-diphenyl-1H-imidazole coupled with three different acceptor moieties such as cyanoacetic acid, rhodanine-3 acetic acid and 4-nitrophenyl acetonitrile, respectively. Interestingly, we observed both dual emission (LE + ICT) and single emission behavior, which was very sensitive to its solvent environments. Effects of solvents on its excited state were probed by lifetime measurements. To verify the influence of different functional groups, we also synthesized D-π-D type compound by replacing acceptor groups with tertiary butyl group and analyzed its solvatochromic behavior. The general and specific solvent effects on optical properties of these compounds were discussed with the help of Lippert–Mataga, Catalán and Kamlet–Taft parameters.

2. Experimental

2.1. Reagents and instruments

All the chemicals were commercially available and they were used without further purification. ^{1}H NMR and ^{13}C NMR were recorded on a Bruker Avance 400 (400 MHz) NMR spectrometer. Dimethylsulfoxide (DMSO-d_6) was used as solvent and tetramethylsilane (TMS) as internal standard. X-ray crystallographic diffraction data were collected on a Bruker SMART APEX-II CCD diffractometer at room temperature using graphite-monochromated Mo Kα radiation (λ = 0.71073 Å). Integration and cell refinement were carried out using Bruker SAINT. The structures were solved by direct methods (SHELXS 86/SHELXS 97) and refined by full-matrix least squares on F^2 using SHELXL 97. All non-hydrogen atoms were refined anisotropically. MERCURY was used for all graphical representation of the results. CCDC reference number 854109 contains the supplementary crystallographic data for the crystal of BIC. UV–vis spectra were recorded at room temperature in quartz cuvettes using JASCO V360 spectrophotometer for hexane, chloroform ($CHCl_3$), ethylacetate (EtOAc), tetrahydrofuran (THF), acetone, acetonitrile (MeCN), methanol (MeOH), N,N-dimethylformamide (DMF) solutions. Fluorescence spectra were obtained from PerkinElmer-LS55 Spectrofluorometer in the above mentioned solvents. Due to poor solubility, qualitative data were only collected in hexane, $CHCl_3$ and EtOAc solvents. Emission spectra were recorded by exciting the molecules in their absorption maximum unless otherwise mentioned. All the experiments were performed at room temperature at a concentration of 10^{-5} M. Quantum yield of the dyes was calculated by following standard procedure using 9,10-diphenylanthracene [37] (Φ_f = 0.95 in ethanol) as reference by using the following equation:

$$\Phi_f = \Phi_R \frac{I_s \times OD_R \times n_s^2}{I_R \times OD_s \times n_R^2} \quad (1)$$

where Φ_R is the fluorescence quantum yield of reference, I is the area under emission spectrum, OD is the optical density at the excitation wavelength and n is the refractive index of solvent. Fluorescence lifetime measurements were carried out in a picosecond time correlated single photon counting (TCSPC) spectrometer. The excitation source is the tunable Ti-sapphire laser (Tsunami, Spectra Physics, USA). The compounds were excited at their maximum absorption (λ_{max}) and monitored at longer wavelength emission (ICT band) in the respective solvents. The fluorescence decay was analyzed by using the software provided by IBH (DAS-6). Transient absorbance to detect triplet properties was performed on air-free solutions if not otherwise specified. The experiments were carried out using nanosecond laser flash photolysis (applied photophysics). The third harmonic (355 nm) of a Q-switched Nd:YAG laser (Quanta-Ray, LAB 150, spectra physics) with 8 ns pulse width and 150 mJ pulse energy was used to excite the samples. The transients were probed using a 150 W pulsed Xenon lamp, a Czerny-Turner monochromator, and Hamamatsu R-928 photomultiplier tube as detector. The transient signals were captured with an Agilent infiniium digital storage oscilloscope, and the data were transferred to the computer for further analysis [38,39].

The multiple linear regression approach of Kamlet–Taft [40] and Catalán [41] new generalized solvent polarity scale (four parameter) has been used to correlate UV–vis absorption and emission energies with an index of the solvent dipolarity/polarizability which is a measure of the solvent's ability to stabilize a charge or dipole through nonspecific dielectric interactions (π^* or SP/SdP), indices of the solvent's hydrogen-bond donor strength (α or SA) and hydrogen-bond acceptor strength (β or SB) according to Eqs. (2) and (3):

$$y_{A,E} = y_0 + a_{\pi^*} \times \pi^* + b_\alpha \times \alpha + c_\beta \times \beta \quad \text{(Kamlet–Taft equation)} \quad (2)$$

$$y_{A,E} = y_0 + a_{SA} \times SA + b_{SB} \times SB + c_{SP} \times SP + d_{SdP} \times SdP \quad \text{(Catalá n equation)} \quad (3)$$

where $y_{A,E}$ denotes a solvent-dependent physicochemical property of absorption and emission in a given solvent and y_0 the statistical quantity corresponding to the value of the property in the gas phase. SP (solvent polarisability), SdP (solvent dipolarity), SA and SB represent independent solvent parameters accounting for various types of solute–solvent interactions. a_{SA}, b_{SB}, c_{SP} and d_{SdP} are adjustable coefficients that reflect the sensitivity of physical property y in a given solvent to the various solvent parameters.

2.2. Synthesis and characterization

As shown in Scheme 1, all the four compounds BIC, BIR, BIN and BIT were synthesized in three steps involving imidazole construction with benzil, ammonium acetate and 4-bromo benzaldehyde in acetic acid followed by Suzuki–Miyaura cross-coupling reaction catalyzed by $Pd[PPh_3]_4$ with 4-formylphenyl boronic acid and 4-tertiary butyl phenyl boronic acid (BIT) followed by Knoevenagel condensation of resulted aldehyde with cyanoacetic acid, rhodanine-3 acetic acid and 4-nitrophenyl acetonitrile and the products obtained in moderate to high yields were characterized well by NMR, MS, and molecular structure of one of the compound (BIC) was confirmed by Single crystal X-ray diffraction analysis. The structures of synthesized compounds are shown in Scheme 2.

2.2.1. Synthesis

*2.2.1.1. 2-(4-Bromophenyl)-4,5-diphenyl-1H-imidazole (**1**).* A mixture of benzil (1.0 g, 4.7 mmol), 4-bromo benzaldehyde (0.87 g,

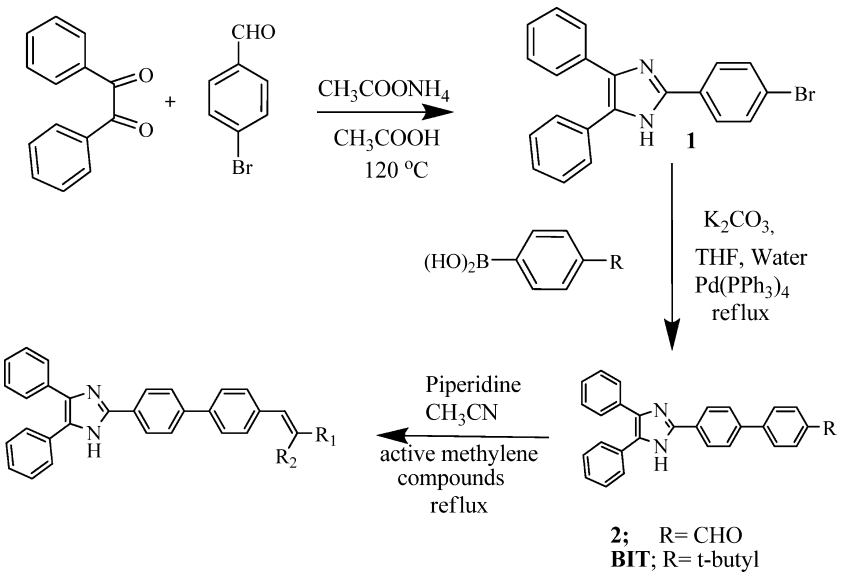

Scheme 1. General synthetic route employed for the preparation of target compounds.

4.7 mmol), ammonium acetate (1.44 g, 18.8 mmol) and glacial acetic acid (30 mL) was heated at 120 °C for 3 h. After cooling to room temperature, the reaction mixture was poured into distilled water with stirring. The separated solid was filtered off, washed with water and dried to give the expected product in good yields. White powder (91%), ^{1}H NMR (DMSO-d_6): δ 7.28 (1H, m), 7.30 (2H, t, 7.2 Hz), 7.37 (1H, m), 7.44 (2H, t, 8 Hz), 7.52 (2H, m), 7.68 (2H, m), 8.02 (2H, m).

*2.2.1.2. 4′-(4,5-Diphenyl-1H-imidazol-2-yl)biphenyl-4-carbaldehyde (**2**).* A solution of compound 1 (1 g, 2.66 mmol), 4-formylphenylboronic acid (0.38 g, 3.2 mmol), $Pd(PPh_3)_4$ (0.15 g, 0.13 mmol) and K_2CO_3 (1.1 g, 7.9 mmol) in THF (50 mL) and water (10 mL) was heated to reflux in an N_2 atmosphere for 12 h. The solution was cooled to room temperature and extracted with dichloromethane. The extracts were dried with anhydrous Na_2SO_4 and concentrated by rotary evaporation. The residue was purified by column chromatography (petroleum ether:EtOAc, 5:1) to obtain the pure product. White powder (75%), ^{1}H NMR (DMSO-d_6): δ 7.23 (1H, t, 7.6 Hz), 7.31 (2H, t, 7.6 Hz), 7.38 (1H, m), 7.45 (2H, d, 8.8 Hz), 7.45 (2H, t, 7.6 Hz), 7.54 (2H, m), 7.92 (2H, d, 8.8 Hz), 8.02 (4H, t, 7.6 Hz), 8.22 (2H, d, 8.8 Hz), 10.06 (1H, s), 12.8 (1H, s). ^{13}C NMR: 125.78, 127.11, 127.21, 127.38, 127.76, 128.39, 130.13, 130.28, 135.08, 138.11, 144.90, 145.08, 192.60.

2.2.1.3. 2-(4′-Tert-butylbiphenyl-4-yl)-4,5-diphenyl-1H-imidazole (BIT). White powder (78%), ^{1}H NMR (DMSO-d_6): δ 1.32 (9H, s), 7.28 (1H, t, 7.2 Hz), 7.31 (2H, t, 7.4 Hz), 7.38 (1H, t, 7.2 Hz), 7.45 (2H, t, 7.2 Hz), 7.51 (4H, m), 7.64 (2H, d, 7.6 Hz), 7.67 (2H, d, 8.4 Hz), 7.77 (2H, d, 8.4 Hz), 8.15 (2H, d, 8.4 Hz), 12.72 (1H, S). ^{13}C NMR: 31.04, 34.20, 125.68, 126.17, 126.61, 128.36, 129.11, 139.54, 145.28 and 150.01.

2.2.1.4. Synthesis of BIC, BIN and BIR. A 15 mL acetonitrile solution of compound 2 (1 mmol), corresponding acceptor groups (1 mmol) and piperidine (0.1 mmol) was refluxed for 12 h under nitrogen atmosphere. The formed precipitate was collected by filtration, washed with acetonitrile and dried under vacuum and then the solid was stirred in water (10 mL) and aq. HCl (1 M, 10 mL) mixture for 1 h. The solid was collected by filtration and dried under vacuum.

2.2.1.5. 2-Cyano-3-[4′-(4,5-diphenyl-1H-imidazol-2-yl)-biphenyl-4-yl]-acrylic acid (BIC). Yellow solid (82%), ^{1}H NMR (DMSO-d_6): δ 7.32 (2H, d, 7.2 Hz), 7.38 (4H, t, 8 Hz), 7.54 (4H, d, 7.6 Hz), 7.93 (2H, d, 8.4 Hz), 8.01 (2H, d, 8.4 Hz), 8.16 (2H, d, 8.4 Hz), 8.22 (2H, d, 8.4 Hz), 8.38 (1H, s); ^{13}C NMR (DMSO-d_6): 103.32, 116.33, 125.79, 127.08, 127.23, 127.77, 128.41, 130.15, 130.60, 131.38, 132.79, 137.94,

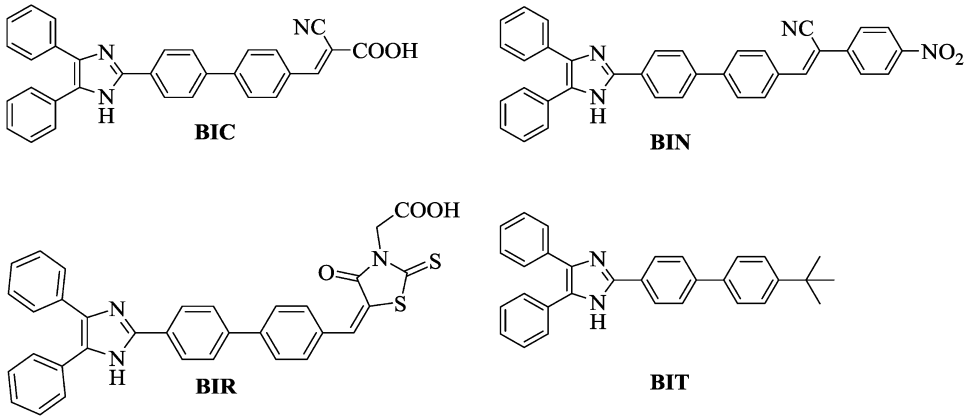

Scheme 2. Structures of the synthesized compounds.

143.56, 144.89, 153.52, 163.35, 147.13. HRMS (ESI) calculated for $C_{31}H_{21}N_3O_2$ $[M+H]^+$ 468.1712. Found *m*/*z*: 468.1759.

2.2.1.6. 2-(5-((4′-(4,5-Diphenyl-1H-imidazol-2-yl)biphenyl-4-yl)methylene)-4-oxo-2-thioxo thiazolidin-3-yl)acetic acid (BIR). Yellowish red solid (73%), ^{1}H NMR (DMSO-d_6): δ 4.76 (2H, s), 7.40 6H, m), 7.54 (4H, d, 7.6 Hz), 7.80 (2H, d, 7.6 Hz), 7.92 (5H, m), 8.24 (2H, d, 7.6 Hz). ^{13}C NMR: 43.64, 125.83, 127.05, 127.32, 127.77, 128.41, 129.96, 131.31, 132.10, 138.10, 141.39, 145.07, 166.74, 193.00, 209.00, 147.13. HRMS (ESI) calculated for $C_{33}H_{23}N_3O_3S_3$ $[M+H]^+$ 574.1259, Found *m*/*z*: 574.1275.

2.2.1.7. 3-[4′-(4,5-Diphenyl-1H-imidazol-2-yl)-biphenyl-4-yl]-2-(4-nitro-phenyl)-acrylonitrile (BIN). Orange solid (76%), ^{1}H NMR (DMSO-d_6): δ 7.24 (1H, d, 7.2 Hz), 7.31 (2H, t, 7.4 Hz), 7.39 (1H, d, 7.2 Hz), 7.45 (2H, t, 7.4 Hz), 7.51 (2H, d, 7.2 Hz), 7.56 (2H, d, 7.2 Hz), 7.92 (2H, d, 8.4 Hz), 7.99 (2H, d, 8.4 Hz), 8.05 (2H, d, 8.8 Hz), 8.12 (2H, d, 8.4 Hz), 8.20 (2H, d, 8.4 Hz), 8.34 (3H, t, 8.8 Hz), 12.79 (1H, s). ^{13}C NMR: 107.72, 117.41, 124.21, 125.70, 126.57, 126.80, 126.84, 127.00, 127.10, 127.79, 127.79, 128.16, 128.35, 128.61, 129.54, 130.02, 130.32, 130.87, 132.18, 135.00, 138.01, 140.03, 142.01, 144.98, 145.61, 147.13. HRMS (ESI) calculated for $C_{36}H_{24}N_4O_2$ $[M+H]^+$ 544.1899. Found *m*/*z*: 544.1878.

2.2.2. Computational methods

To elucidate the optical and electronic properties of the molecule, theoretical calculations have been performed on the imidazole fluorophore. The geometries of the molecule were fully optimized at the DFT level using the B3LYP [42–45] functional (Becke's three-parameter hybrid functional using the LYP correlation functional) at the 6-311G(d,p) basis set. The excited-state geometries were optimized by the ab initio configuration interaction singles method (CIS) [46]. These fully optimized stationary points were further characterized by harmonic vibrational frequency analysis to ensure that all the structures are minima on the potential energy surface. The electronic absorption and emission spectra, both in vacuum and in solvent, were carried out using the time-dependent density functional theory (TDDFT) [47,48] method CAM-B3LYP/6-311G(d,p) [49] using the optimized ground and excited structures, respectively. The solvent effect has been included by the polarized continuum model (PCM) [50]. The program used to perform the calculations was the Gaussian 09W [51].

3. Results and discussion

3.1. Crystal structure

The molecular structure of BIC was determined by single crystal X-ray crystallography. Figure S1 illustrates the molecular packing feature of BIC crystal, and the ORTEP view of the crystal is shown in Fig. 1. Interestingly, the molecule is arranged in a zig-zag like structure along *c* axis (Fig. S1). The compound is crystallized in a monoclinic crystal system in the *P*21/*c* space group. The torsion angle between the imidazole ring and C4-phenyl ring (77.2)° suggests that the phenyl ring is more twisted. On the other hand, the torsional angle values of phenyl ring at C5 (6.6)° and C2 (32.0)° suggest that the molecular frame work of the phenyl groups (C2 and C5) are twisted slightly; hence, the π-conjugation will not be much affected (Fig. 1). Similarly, the spacer biphenyl group (42.2)° and the phenyl group attached with acceptor group (21.03)° also less twisted. Hence, the π-conjugation from imidazole moiety toward the acceptor moiety will not be disturbed. Likewise, the bond angles of benzene ring and five member ring are close to 120° and 108° suggest that the π electrons in the whole molecule are delocalised. The relevant crystal data of BIC are presented in SI Table 1.

3.2. UV–vis absorption spectra

To gain insight into the photophysical processes in these compounds, efforts have been taken to investigate their absorption and emission behaviors in different solvents. The spectral data of all the compounds in various solvents are reported in Table 1. From Fig. 2A, the absorption band at 279 nm in BIT is attributed to the π–π* transition arising from the phenyl groups attached at C4 and C5 position of imidazole ring. The band at 329 nm is attributed to the π–π* transition arising from biphenyl group attached to C2 position [52]. Moreover, the effect of solvent polarity (from nonpolar to polar) on the absorption behavior is very minimal about 10 nm (Fig. 2A). On the other hand, replacing tertiary butyl moiety in BIT with various acceptor moieties results in enhanced bathochromic shift; in addition, the spectral behavior is very sensitive to solvent polarity. In BIC, tuning of solvent polarity from hexane to THF results in a large bathochromic shift (Fig. 2B) of about 55 nm. Conversely, the negative solvatochromism observed in MeOH and MeCN could be attributed to the hydrogen bonding interaction of solvent molecules with imidazole ring. This typical behavior can be ascribed to the hydrogen-bonding interactions, which probably retard the reorientation of the fluorophore by hindering the rotation of the aryl unit [53,54]. The highly sensitive peaks around 330–390 nm in different solvents suggest that the band arises because of intramolecular charge transfer between the donor imidazole moiety to the acceptor cyanoacrylic acid. Further, it can be evidenced from the results obtained from binary solvent absorption spectral measurements. For instance, upon titration of THF solution of BIC with water, interestingly we have observed a significant blue shift of 30 nm (for 20% water) as shown in Fig. 2C. On further titration, no remarkable change has been observed in the absorption wavelength. From the observed result, it can be evidenced that the increasing percentage of water content in the THF solution induces the hydrogen bonding interaction which may diminish the electron withdrawing nature of acceptors groups and/or retard the reorientation of the molecule by hindering the rotation of the aryl unit.

By the same token, replacement of cyanoacrylic acid in BIC by other acceptors such as rhodanine-3-acetic acid (BIR) and 4-nitrophenylacetonitrile (BIN) leads to bathochromic shift of λ_{max} by 56 nm and 27 nm (SI Figs. 2 and 3) while changing the polarity of the environment from non-polar to polar. The charge transfer efficiency of the compounds based on λ_{max} follows the order BIC < BIN < BIR. It could be attributed to the presence of two strong electron withdrawing groups (—CN and —NO_2) in BIN and additional electron withdrawing groups such as ketone and thione with —COOH in BIR results in very high bathochromic shift. The extinction coefficients of the charge-transfer bands (Table 1) in these compounds are moderate to high ranging from ~11,000 to ~60,000 M^{-1} cm^{-1}.

3.3. Fluorescence emission and excitation spectra

More notably, the emission spectra of all the compounds show remarkably strong solvatochromic red shifts on going from nonpolar hexane to polar DMF (Table 1). It is noticeable that the effect of polarity of the medium on the emission behavior is more pronounced than that of the absorption behavior. This observation suggests that the emitting states of the compounds are more polar than the ground state. This effect is typical for an ICT transition within the fluorophores [55]. As shown in Fig. 3A, BIC exhibited single emission behavior in hexane, THF, acetone, $CHCl_3$ and DMF and dual emission in MeOH, EtOAc, MeCN solutions. In hexane, Stokes shift is very small, about 4213 cm^{-1} which could be attributed to the LE → S_0 transition and the emission behavior is independent of excitation wavelength. On increasing the polarity

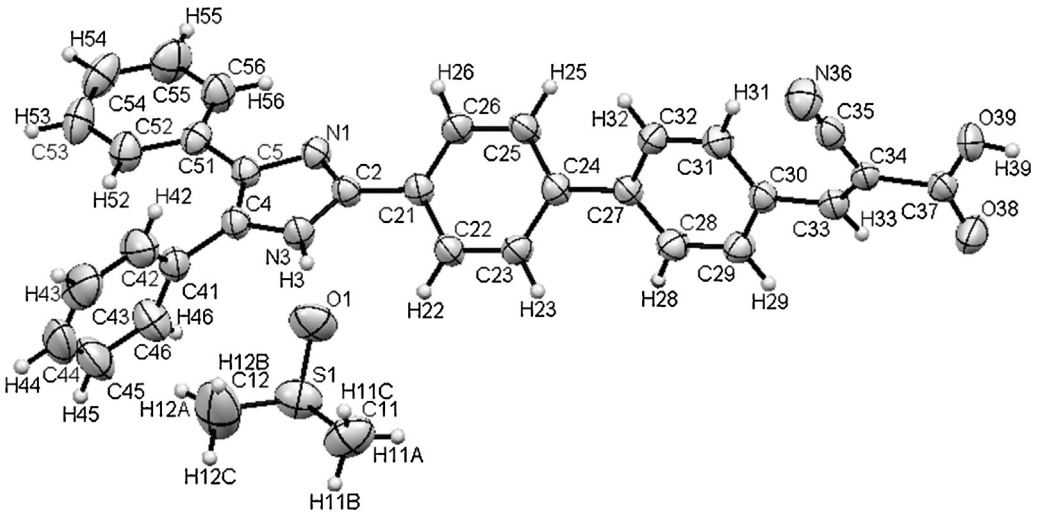

Fig. 1. X-ray molecular structure of BIC showing thermal ellipsoids of 50% probability. Solvent DMSO also present in the crystal structure.

Table 1
Relevant data from absorption and emission curves of the compounds in solvents with different polarity.

	λ_{max}^{abs} nm			$\varepsilon \times 10^3\ M^{-1}\ cm^{-1}$			λ_{max}^{em} nm			$\Delta\nu\ (cm^{-1})$		
	BIC	BIN	BIR	BIC	BIN	BIR	BIC	BIN	BIR	BIC	BIN	BIR
Hexane	332	–	357	–	–	–	386	–	401	4213	–	3073
$CHCl_3$	358	374	398	–	–	–	443	443	445	5359	4164	2653
EtOAc	382	394	408	–	–	–	428, 555	493	572	8159	5096	7027
THF	387	398	413	37.5	60.4	54.0	554	494	570	7789	4882	6669
Acetone	369	392	408	54.0	60.5	12.6	520	444, 518	432, 506	7869	6205	4746
MeOH	357	381	400	51.9	–	43.4	415, 524	424, 509	446, 516	8927	6600	5620
MeCN	352	386	400	11.9	40.7	35.0	424, 528	436, 528	457, 508	9469	6967	5314
DMF	361	401	406	43.7	39.9	46.2	524	453, 520	532	8470	5706	5833

of the medium, ICT transition is more prominent than the LE transition which resulted in large red shifted emission. Furthermore, the emission behavior is also independent of different excitation wavelengths (SI Figs. 15 and 16). On the contrary, the observed dual emission behavior, peak intensity and peak position are very sensitive to the excitation wavelength in MeOH, EtOAc and MeCN (for example, see SI Figs. 8 and 9). LE transition around 424 nm is more prominent on higher energy excitation while ICT transition around 550 nm is more prominent on lower energy excitation. Comparing the results, the Stokes shift increases on increasing the polarity of the solvents and decreases rapidly in polar protic solvents. The observed results suggest that the Stokes shift of the compound in different solvents is governed by three factors: solvent polarity, hydrogen bonding and ICT. It is expected that the compounds can have both the hydrogen-bonding interaction as well as ICT in MeOH and MeCN and the latter is more prominent in other solvents. The emission spectra of BIC in binary solvent mixture (water in THF) also confirm the above discussions. From Fig. 3B, we observed significant change on increasing the percentage of water in THF solution of BIC. In pure THF, the emission from ICT has only been observed. On increasing the percentage of water, the ICT emission around 530 nm was diminished while the new emission peak around 430 nm was generated. At 20% of water in THF solutions, the major emission from LE transition was only observed. The observed result supports the dual emission behavior is completely governed by the solvent environment. Subsequently, this remarkable feature has also been evidenced by comparing the emission behavior of BIT. Fig. 3C depicts the emission spectra of BIT in different solvents with varying polarity. Single emission behavior with the independent nature of emission spectra on different excitation wavelength suggests that the observed band is attributed to the normal LE → S_0 transition. The bathochromic shift of 26 nm observed on varying polarity of the solvents can be ascribed to the general solvent effect. Moreover, no ICT emission was observed which is due to the absence of acceptor groups.

As evidenced earlier for BIC, BIN also exhibited the excitation energy dependant dual emission (SI Fig. 10A) and ICT behavior in MeCN and EtOAc solutions. In DMF, a peak was broadened on higher energy excitation; however, no distinct dual emission was observed. The emission spectrum of BIR in different solvents is shown in SI Fig. 10B. The justification for the dual emission (in MeOH and MeCN) and ICT behavior of BIR in different solvents can be correlated with the discussion of BIC and BIN. However, excluding hexane and $CHCl_3$, the emission behavior is highly dependent on excitation wavelength in other polar solvents. It can be attributed to the availability of more number of functional groups that will enhance the possibility to form more rigid solvation cage due to hydrogen bonding with solvents. Hence, it can experience two different local environments in the ground state itself. It can be analyzed from emission wavelength dependant excitation spectra measurements. In which, we observed two different excitation spectral behavior on changing the emission wavelength (SI Fig. 11) from higher energy to lower energy confirms the presence of two different local environments.

3.4. Optimized geometry and frontier molecular orbital analysis

The optimized ground-state geometries of the synthesized compound are shown in SI Fig. 14. Selected bond lengths compared with the experimental data are shown in SI Table 2. The C—C bond length in all the compounds is about 1.34–1.48 Å, suggests that

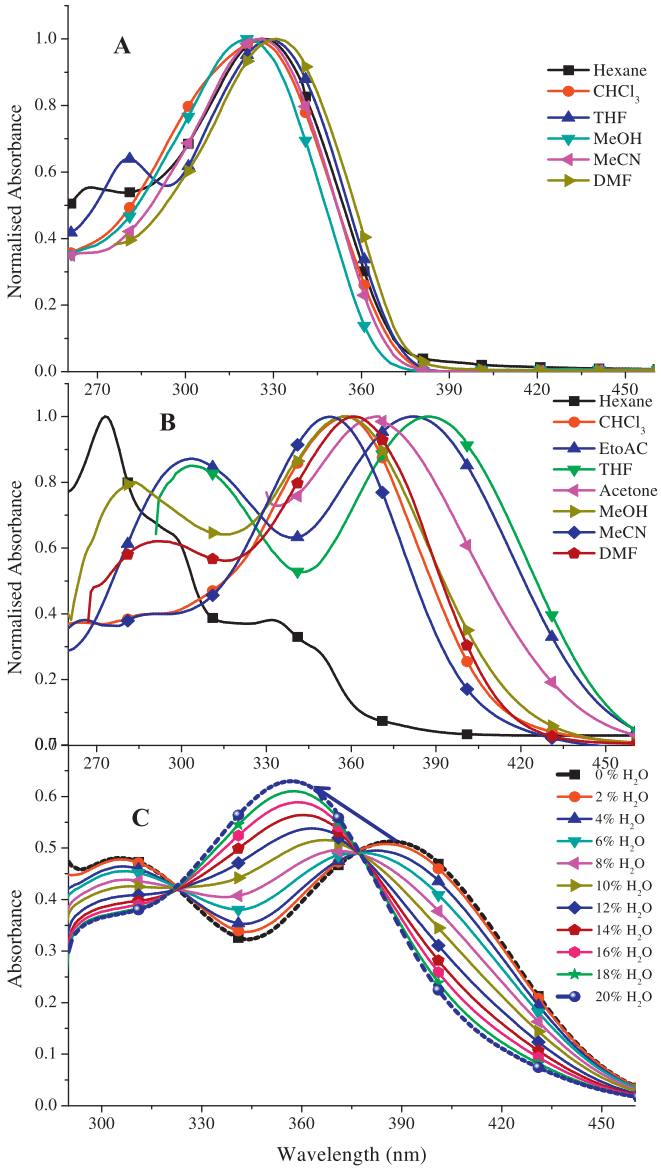

Fig. 2. Normalized absorption spectra of BIT (A) and BIC (B) in solvents with different polarity. Absorption spectra of BIC in THF–water (C) solvent system.

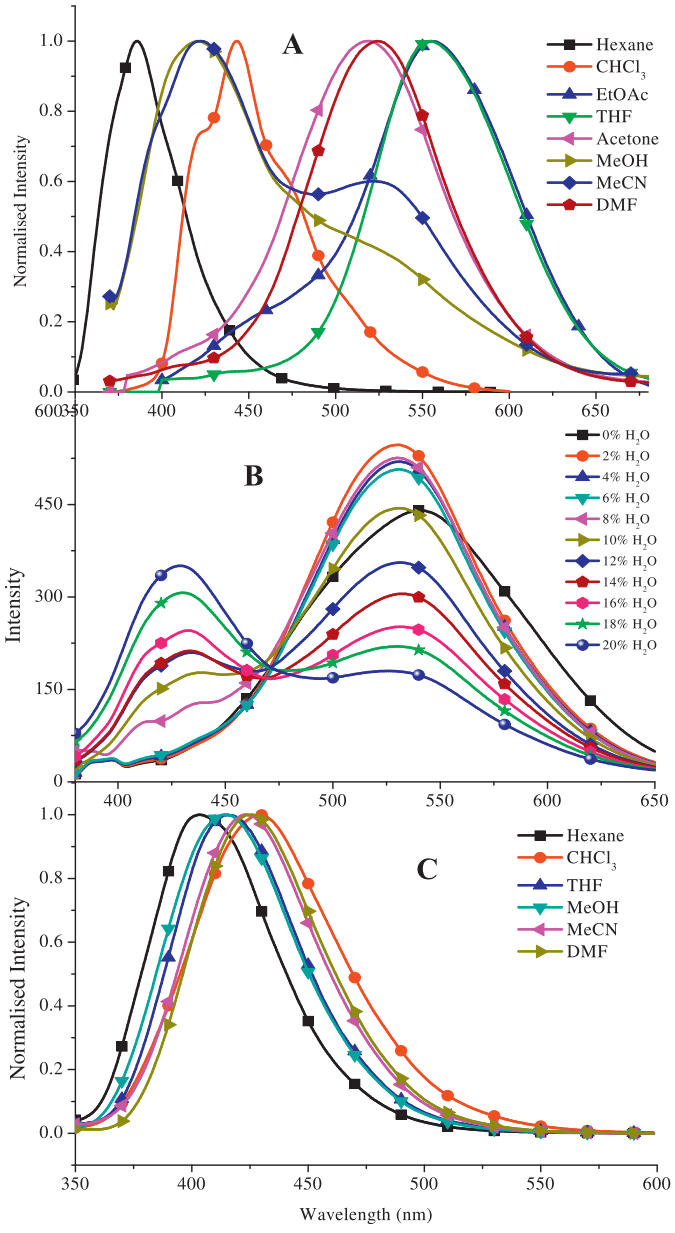

Fig. 3. Normalized emission spectra of BIC (A) and BIT (C) in solvents with different polarity. Emission spectra of BIC in THF–water (B) solvent system.

the π electrons are delocalized over the entire molecule. For the sake of characterizing the optical and electronic properties of the molecule, it is useful to examine the highest occupied molecular orbitals (HOMOs), lowest unoccupied molecular orbitals (LUMOs) and band gaps (HOMO–LUMO gap). The relative ordering of the HOMO and LUMO orbitals provide a realistic indication in the excitation properties. From Fig. 4, it is interesting to note that the HOMO of BIC, BIN and BIR is localized on the donor part, while the LUMO is mainly centered on the acceptor part. On the other hand LUMO+1, LUMO+2, HOMO−1 orbitals are predominantly localized on the π-spacer and acceptor unit, while HOMO−2 of BIC, BIN is localized on the donor phenyl part and BIR is an acceptor part. This indicates that the HOMO → LUMO transition bear a significant ICT character and the other absorption bands have dominant contributions HOMO → LUMO+1 and HOMO → LUMO+2 and are mainly $\pi \rightarrow \pi^*$ character. The energy gaps of compounds BIC, BIN and BIR are found to be 2.7, 2.53 and 2.63 eV, respectively. The donor centered HOMO levels for compounds BIC, BIN and BIR are observed in the range of −5.61, −5.62 and −5.55 eV, respectively. The acceptor centered LUMO levels for them are in the range of −2.87, −3.09 and −2.92 eV. The increasing order of band gap is as follows: BIN < BIR < BIC.

In addition to the above, the molecular orbitals are often used to relate the spectral properties of molecules and provide decisive clues for synthesizing newer molecules. Therefore it is essential to identify and understand the nature of various segments of the molecule and their individual contributions toward HOMOs and LUMOs. Hence the contributions of various fragments of the molecules have been computed using QMForge [56] program. The whole molecule has been segmented into three fragments, namely donor, π-spacer and acceptor units and their corresponding percentage contributions are summarized in Table 2. As evident from the molecular orbital diagrams, HOMOs are majorly centralized by donor (80%) and interestingly LUMOs are majorly stabilized by acceptor (78%). This indicates that the donor and acceptor parts in BIC, BIN and BIR are responsible for the intramolecular charge transfer upon excitation.

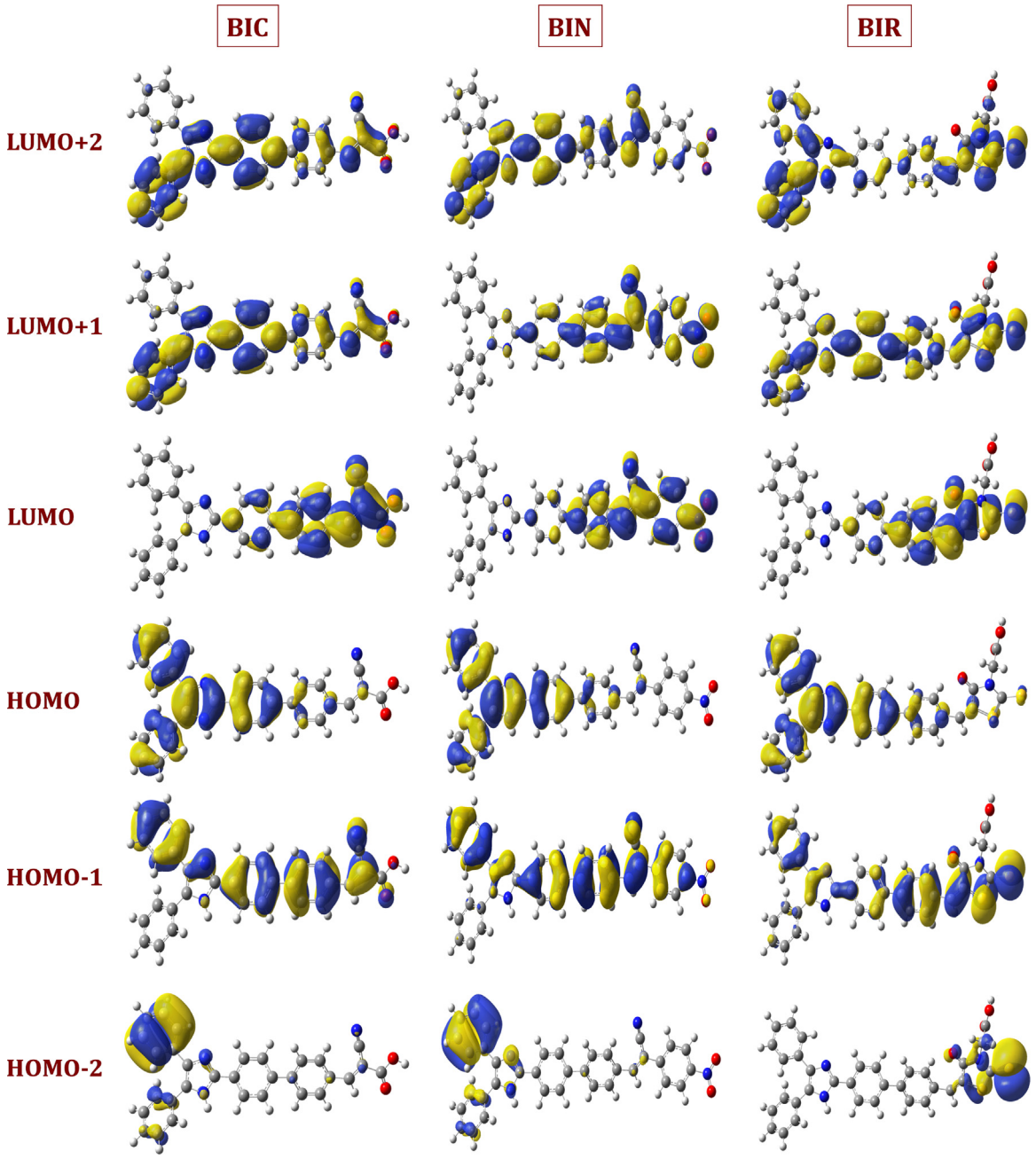

Fig. 4. FMO pictures of BIC, BIN and BIR.

3.5. Computed absorption and emission spectra

To understand electronic transitions of the synthesized compounds, TDDFT calculations on the absorption and emission spectra in both vacuum and solvent (MeCN) were performed. The electronic absorption and emission spectra were calculated using the TD-DFT method to rationalize the nature of electronic transitions and the contributing configurations. The calculated wavelengths from absorption and emission spectra, excitation wavelength, main transition configurations and oscillator strengths for the most relevant singlet excited states of BIC, BIN and BIR are summarized in Tables 3 and 4, respectively.

From Table 3 and the MOs in Fig. 4, the experimental band found at 352 nm for BIC corresponds to the transition predicted at 361 nm, and this originates from HOMO → LUMO transition with ICT character (62%). Another band exhibited at 265 nm mainly originates from HOMO → LUMO+2, HOMO → LUMO+1 and HOMO → LUMO, which assigned as $\pi \rightarrow \pi^*$ transition (37%, 29% and 18%, respectively). As for BIN, the experimental absorption band of 386 nm at longer wavelength is of ICT character that corresponds to the transition calculated at 371 nm, which originates from HOMO → LUMO (41%). Another band exhibited at 286 nm mainly originates from HOMO → LUMO+2, HOMO → LUMO+3 and

Table 2
Molecular orbital composition (%) in the ground state for BIC, BIN and BIR.

Molecule	HOMO			LUMO		
	Donor	π-Spacer	Acceptor	Donor	π-Spacer	Acceptor
BIC	79.89	18.61	1.49	3.41	40.56	56.02
BIN	78.74	19.20	2.06	1.45	20.43	78.12
BIR	75.20	20.38	4.42	2.14	25.97	71.90

Table 3
Electronic transition data obtained by TD-DFT (λ_{abs}) for BIC, BIN and BIR at the CAM-B3LYP/6-311G(d,p) optimized geometry.

Molecule	States	Expt. λ_{abs} (nm)	Cal. λ_{abs} (nm)	Oscillator strength f	E (eV)	Major contribution
BIC	Gas-phase		354.6	1.6077	3.50	HOMO → LUMO (65%) HOMO−1 → LUMO (20%) HOMO → LUMO+1 (10%)
			262.3	0.3734	4.73	HOMO → LUMO+2 (48%) HOMO → LUMO+1 (22%) HOMO → LUMO (12%)
	MeCN	352	361.1	1.7687	3.43	HOMO → LUMO (62%) HOMO−1 → LUMO (24%) HOMO → LUMO+1 (9%)
			264.8	0.4644	4.68	HOMO → LUMO+2 (37%) HOMO → LUMO+1 (29%) HOMO → LUMO (18%)
BIN	Gas-phase		366.0	2.0214	3.39	HOMO → LUMO (49%) HOMO−1 → LUMO (30%) HOMO → LUMO+1 (9%)
			287.7	0.3405	4.31	HOMO → LUMO+2 (41%) HOMO → LUMO (23%) HOMO → LUMO+3 (9%)
	MeCN	386	370.9	2.2191	3.34	HOMO → LUMO (41%) HOMO−1 → LUMO (36%) HOMO → LUMO+1 (11%)
			286.2	0.3394	4.33	HOMO → LUMO+2 (35%) HOMO → LUMO+3 (27%) HOMO → LUMO (21%)
BIR	Gas-phase		381.0	1.5968	3.25	HOMO−1 → LUMO (39%) HOMO → LUMO (37%) HOMO−2 → LUMO (10%)
			269.9	0.4365	4.59	HOMO → LUMO+3 (36%) HOMO → LUMO+1 (21%) HOMO → LUMO (10%) HOMO → LUMO+2 (10%)
	MeCN	400	390.8	1.9800	3.17	HOMO−1 → LUMO (50%) HOMO → LUMO (42%)
			273.5	0.4107	4.53	HOMO → LUMO+3 (31%) HOMO → LUMO+1 (23%) HOMO → LUMO (14%)

HOMO → LUMO (35%, 27% and 21%, respectively), which can be assisted as $\pi \rightarrow \pi^*$ transition. Similarly, concerning BIR the experimental band found at 400 nm corresponds to the transition calculated at 391 nm with larger oscillator strengths is ICT character of HOMO → LUMO (50%) transition. Another band exhibited at 273 nm is $\pi \rightarrow \pi^*$ transition, and originates from HOMO → LUMO+3, HOMO → LUMO+1 and HOMO → LUMO (31%, 25% and 14%, respectively). Theoretical emission spectra for imidazole fluorophores based on optimized excited-state geometries are presented in Table 4. The emission peaks in MeCN solvent, with the largest oscillator strength for the compounds BIC, BIN and BIR are due to LUMO → HOMO transition. The calculated absorption and emission bands are in good agreement with the experimental results.

Overall, the DFT and TDDFT calculations reveal deeper insights into the electronic structures, and optical properties and the nature of transition of the synthesized molecules are well explored by our theoretical methods.

3.6. Solvatochromic measurement and dipole moments

The extent of charge separation on electronic excitation of compounds were quantified by measuring the change in the dipole moment ($\Delta\mu = \mu_e - \mu_g$) utilizing the shift between the absorption and emission maxima $\Delta\nu = (\nu_{abs} - \nu_{em})$ as a function of solvent polarity. According to the Lippert–Mataga [57] equation (4).

$$\nu_{abs} - \nu_{em} = \Delta\nu = \frac{2}{hca^3}(\mu_e - \mu_g)^2 \Delta f + \text{Constant} \quad (4)$$

Table 4
Emission data obtained by TD-DFT for BIC, BIN and BIR at the CIS/6-31G(d,p) optimized geometry.

Molecule	States	Expt. λ_{em} (nm)	Cal. λ_{em} (nm)	Oscillator strength f	E (eV)	Major contribution
BIC	Gas-phase		414.6	1.9400	2.99	LUMO → HOMO (82%) LUMO → HOMO−1 (10%)
	MeCN	424	432.1	2.0606	2.87	LUMO → HOMO (81%) LUMO → HOMO−1 (12%)
BIN	Gas-phase		432.4	2.2166	2.87	LUMO → HOMO (70%) LUMO → HOMO−1 (23%)
	MeCN	436	447.3	2.3241	2.77	LUMO → HOMO (69%) LUMO → HOMO−1 (23%)
BIR	Gas-phase		468.0	1.5113	2.65	LUMO → HOMO (71%) LUMO → HOMO−1 (24%)
	MeCN	457	487.0	1.6119	2.55	LUMO → HOMO (67%) LUMO → HOMO−1 (28%)

Table 5
Estimated from Eq. (3) coefficients (y_o, a_{SA}, b_{SB}, c_{SP}, d_{SdP}), their correlation coefficients (r) for the multiple linear regression analysis of $E(A)$, $E(F)$ and $E(S)$ of the compounds as a function of the Catalán four-parameter solvent scale.

	y	y_o (kcal/mol)	a_{SA}	b_{SB}	c_{SP}	d_{SdP}	r
BIC(LE)	E_{abs}	95.03(±15.32)	3.86(±7.34)	−13.28(±7.14)	−13.77(±23.03)	0.39(±5.40)	0.8119
	E_{emi}	106.4(±26.61)	13.08(±12.75)	−21.26(±12.41)	−49.0(±40.0)	−3.78(±9.38)	0.8767
	E_{st}	12.95(±29.73)	−9.21(±14.24)	7.98(±13.86)	35.23(±44.23)	4.17(±10.48)	0.7045
BIC(ICT)	E_{emi}	66.15(±18.84)	6.21(±9.03)	−20.76(±8.79)	10.59(±28.32)	−11.62(±6.64)	0.9359
	E_{st}	26.94(±10.16)	−2.34(±4.87)	7.48(±4.74)	−24.36(±15.27)	12.01(±3.58)	0.9582
BIN(LE)	E_{abs}	79.35(±1.88)	4.75(±0.63)	−8.23(±0.64)	−2.09(±2.27)	−1.59(±0.73)	0.9956
	E_{emi}	53.37(±7.41)	8.58(±2.49)	−10.91(±2.54)	3.37(±8.96)	14.05(±2.90)	0.9834
	E_{st}	25.98(±5.57)	−3.83(±1.87)	2.67(±1.91)	−5.47(±6.74)	−15.64(±2.18)	0.9853
BIN(ICT)	E_{emi}	54.90(±6.0)	5.44(±2.01)	−7.33(±2.05)	12.60(±7.25)	−13.06(±2.43)	0.9880
	E_{st}	24.44(±4.73)	−0.69(±1.38)	−0.90(±1.41)	−24.69(±4.99)	11.47(±1.61)	0.9915
BIR(LE)	E_{abs}	86.88(±9.75)	1.71(±4.67)	−6.51(±4.55)	12.78(±14.66)	−5.60(±3.43)	0.9103
	E_{emi}	98.61(±26.36)	7.38(±12.63)	−31.82(±12.29)	−45.30(±39.63)	6.29(±9.29)	0.8745
	E_{st}	11.73(±23.22)	−5.67(±11.12)	25.30(±10.83)	32.52(±34.90)	−11.89(±8.19)	0.8316
BIR(ICT)	E_{emi}	70.24(±18.36)	5.66(±8.79)	−25.20(±8.56)	0.12(±27.59)	−5.17(±6.47)	0.9285
	E_{st}	16.63(±11.98)	−3.95(±5.74)	18.68(±5.59)	−12.90(±18.01)	−0.41(±4.22)	0.9204

where

$$\Delta f = \frac{\varepsilon - 1}{2\varepsilon + 1} - \frac{n^2 - 1}{2n^2 + 1} \quad (5)$$

where $\Delta\nu$ is the Stokes shift, μ_g and μ_e are ground and excited state dipole moments, c is the speed of light, h is the Planck's constant, and a is the Onsager cavity radius swept out by the fluorophore. A plot of $\Delta\nu$ versus Δf gives $\Delta\mu$ from the slope. Using the mole inspiration software, the volume of the compounds is measured. By using the volume, Onsager cavity radius 4.65 Å (BIC), 4.88 Å (BIN) and 4.88 Å (BIR) has been calculated. From the DFT calculations at the B3LYP/6-311G(d,p) level, the ground state dipole moment (μ_g) is obtained. The values of μ_g for compounds BIC, BIR and BIN are 6.87, 6.04 and 9.29 D, respectively. The positive slope of the Lippert–Mataga plot in the solvents studied suggests that general solvent effects are responsible for the observed positive solvatochromic shifts in emission. The dipole moment change on excitation is estimated from the slope of Eq. (4) to be around 19.21, 16.65 and 21.39 D for BIC, BIR and BIN (for ICT band), respectively, which is higher than the μ_e (LE band) values (15.90, 10.36 and 19.43 D for BIC, BIR and BIN, respectively). Substantially, high values of μ_e (ICT) than μ_e (LE) thus obtained from plot suggest that the fluorescence states of all these compounds are of strong ICT character [58].

3.7. Multi-linear regression analysis

Multi-parameter correlation is an excellent and preferable method to analyze the various factors affecting the photophysical properties of the compounds and which has been applied successfully to various physicochemical parameters [59]. The most frequently used solvent scales are those of Kamlet–Taft, and Catalán. The new four-parameter Catalán solvent scale has an advantage over other solvent scales. Hence, herein the spectral and photophysical parameters of the compounds studied in all solvents used will be discussed based on the four-parameter Catalán solvent scale (Table 5). However, the correlations obtained using Kamlet–Taft solvent scale are also presented (Table 6) and will be compared with each other.

Table 5 compiles the estimated regression coefficients y_o, a_{SA}, b_{SB}, c_{SP}, d_{SdP} and the correlation coefficients (r) for the multilinear regression analysis of the maxima of absorption (E_{abs}) and emission (E_{emi}) of the compounds according to Eq. (3) for all the solvents studied. Use of the solvent parameters set (SA, SB, SP and SdP) gives fair fits to E_{abs} using r as a goodness-of-fit criterion (r = 0.8119 for BIC, 0.9956 for BIN and 0.9103 for BIR). Moreover, the analysis of the E_{abs} data of the compounds to the popular Kamlet–Taft solvent scales (Table 6) using the (α, β, π^*) parameters showed fair fits (but slightly lower than Catalán treatment) as assessed by the values of r (0.7605 for BIC, 0.6912 for BIN and 0.9172 for BIR).

Table 6
Correlation of $E(A)$, $E(F)$ and $E(S)$ with Taft's π^* (solvent dipolarity/polarisability), α and β (hydrogen bond donating and accepting ability of the solvent) values based on multiple linear regression analysis (Kamlet–Taft).

	y	y_o (kcal/mol)	$a\alpha$	$b\beta$	$c\pi^*$	r
BIC(LE)	E_{abs}	84.48(±2.90)	4.64(±4.17)	−16.11(±11.05)	−1.80(±7.93)	0.7605
	E_{emi}	74.70(±4.87)	14.19(±7.00)	−31.14(±18.54)	−0.32(±13.30)	0.8562
	E_{st}	9.78(±5.27)	−9.54(±7.58)	15.03(±20.06)	2.13(±14.40)	0.6744
BIC(ICT)	E_{emi}	71.10(±5.16)	−1.36(±7.42)	−10.17(±19.65)	−15.58(±14.10)	0.8244
	E_{st}	13.38(±3.01)	6.01(±4.33)	−5.94(±11.46)	17.39(±8.22)	0.8677
BIN(LE)	E_{abs}	78.65(±4.77)	2.66(±2.38)	−6.75(±6.59)	−3.35(±6.74)	0.6912
	E_{emi}	55.62(±7.27)	8.75(±3.63)	−10.85(±10.04)	17.03(±10.26)	0.8376
	E_{st}	23.01(±3.28)	−6.09(±1.64)	4.09(±4.53)	−20.44(±4.64)	0.9508
BIN(ICT)	E_{emi}	68.58(±8.94)	−4.05(±4.48)	3.75(±12.39)	−20.33(±12.67)	0.7061
	E_{st}	9.05(±4.32)	6.72(±2.16)	−10.51(±5.97)	16.99(±6.10)	0.9083
BIR(LE)	E_{abs}	78.49(±1.60)	1.31(±2.30)	−7.25(±6.09)	−6.38(±4.37)	0.9172
	E_{emi}	70.15(±6.10)	12.30(±8.77)	−34.63(±23.21)	6.31(±16.66)	0.7529
	E_{st}	8.34(±5.45)	−10.99(±7.84)	27.37(±20.76)	−12.70(±14.90)	0.6437
BIR(ICT)	E_{emi}	69.15(±5.31)	1.73(±7.64)	−18.64(±20.23)	−6.93(±14.52)	0.7761
	E_{st}	9.33(±4.32)	−0.42(±6.21)	11.38(±16.43)	0.55(±11.79)	0.5632

Table 7
Quantum yield (Φ_f), lifetime (τ), average lifetime ($\langle\tau\rangle$), radiative (k_r) and nonradiative (k_{nr}) rate constants of the compounds in different solvents.

	BIC					BIN					BIR				
	THF	Acetone	MeOH	MeCN	DMF	THF	Acetone	MeOH	MeCN	DMF	THF	Acetone	MeOH	MeCN	DMF
τ_1 (ns)	1.46	1.39	1.15	1.19	1.12	1.47	1.48	1.08	0.90	1.32	0.85	1.05	1.07	0.82	0.79
α_1 (%)	21	44	39	42	37	25	16	48	26	48	40	41	31	32	28
τ_2 (ns)	3.21	2.48	4.05	1.78	1.16	2.33	2.53	2.95	2.39	2.50	2.01	2.47	3.35	2.13	1.97
α_2 (%)	79	56	61	58	63	75	84	52	74	52	60	59	69	68	72
χ^2	1.07	1.19	1.22	1.18	1.19	0.93	0.92	1.08	1.15	1.22	1.00	1.10	1.14	1.24	1.21
$\langle\tau\rangle$ (ns)	2.09	2.04	3.59	1.58	1.45	2.18	2.42	2.47	1.59	1.99	1.75	2.14	2.40	1.92	1.80
Φ_f	0.49	0.50	0.15	0.40	0.55	0.11	0.18	0.07	0.15	0.17	0.18	0.19	0.09	0.17	0.22
k_r (10^8 s^{-1})	2.33	2.45	0.41	2.52	3.77	0.50	0.74	0.28	0.94	0.85	1.02	0.88	0.37	0.88	1.21
k_{nr} (10^8 s^{-1})	2.43	2.45	2.36	3.78	3.08	4.08	3.38	3.75	5.32	4.16	4.67	3.78	3.78	4.31	4.32

It is striking that the notable solvent-dependant spectral shifts can be described so well by the new Catalán solvent scales. The advantage of this generalized treatment of the solvent effect is that it allows one to split up the relative contribution of dipolarity, polarizability, acidity and basicity of the medium. By contrast, in the Kamlet–Taft approach, the solvent parameter π^* contains both (solvent dipolarity and polarizability) effects, and hence this latter methodology can never be used to entangle solvent polarizability and dipolarity effects.

Herein, the Catalán methodology is used to unravel which solvent properties are primarily responsible for the observed spectral shifts. The estimated high b_{SB} (13.28 for BIC and 6.51 for BIR) and c_{SP} (13.77 for BIC and 12.78 for BIR) values compared to the a_{SA} and d_{SdP} in the analysis of E_{abs} of BIC and BIR indicate that the small change in E_{abs} principally reflected a change in basicity and polarizability of the environments. Conversely, for BIN, the change in E_{abs} arises not solely from solvent basicity (b_{SB} is 8.23) of the environment. Similar dependences also observed from the correlation of (E_{abs}) with the three-parameter solvent polarity scales, where the contribution of solvent basicity (Table 6) is higher than the other parameters.

Next we examined which solvent characteristics account for the shift of E_{emi} in LE and ICT band. As observed for E_{abs}, fair fits were also found for the multilinear analysis of E_{emi} (for both LE and ICT) data of the compounds accordingly to Eq. (3). Among them, E_{emi} (ICT) fits much better than E_{emi} (LE). Indeed, the r values for E_{emi} (LE) found were 0.8767 for BIC, 0.9834 for BIN, 0.98745 for BIR which is higher for E_{emi} (ICT) like 0.9359 for BIC, 0.9880 for BIN, 0.9285 for BIR. The Kamlet–Taft treatment has much lower fit values ranging from 0.7529 to 0.8562 for the studied compounds. The relatively large b_{SB} and c_{SP} value of BIC and BIR in E_{emi} (LE) band reveals that the solvent basicity and polarisability plays a major role in governing LE band of emission spectra. Conversely, for E_{emi} (ICT), remarkable contribution from solvent dipolarity (d_{SdP}) implies that the observed large bathochromic shift is due to the change in the solvent dipolarity of the medium. Obviously, solvent dipolarity plays major role on excited state of the molecules than the polarizability does, which is a reason for strong red shift [59]. For BIN, solvent dipolarity (both LE and ICT) solely plays a major role on shifting the spectral behavior in excited state than the acidity, basicity and polarisability. As evidenced from Catalán approach, Kamlet–Taft methodology also revealed that the dipolarity/polarizability (π^*) of the environment is the major factor which affects E_{emi} values of the compounds (Table 6).

3.8. Quantum yield and time-resolved fluorescence analysis

Fluorescence quantum yields (Φ_f) of the compounds were measured in solvents of different polarity and are presented in Table 7. Because of high polar nature, the compounds are not completely soluble in less polar solvents (hexane, $CHCl_3$, EtOAc). Hence, the quantum yields in these solvents are not calculated. Fluorescence quantum yields are found to be increased with the increase in solvent polarity. This clearly indicates a highly polar emissive state. However, it is decreased in MeOH, which may be due to protic solvent–solute interactions [60]. Φ_f values are decreased with increase in the strength of acceptor groups. For instance, BIC showed Φ_f values of around 0.40–0.55 exclude MeOH. But, BIN and BIR showed significant decrease in Φ_f values to be 0.09–0.22.

To interpret the photophysical properties in a more intuitive manner, the fluorescence lifetimes of the compounds were measured in different solvents. Thus, fluorescence decay traces of the compounds (Fig. 5A–C) in different solvents were collected as

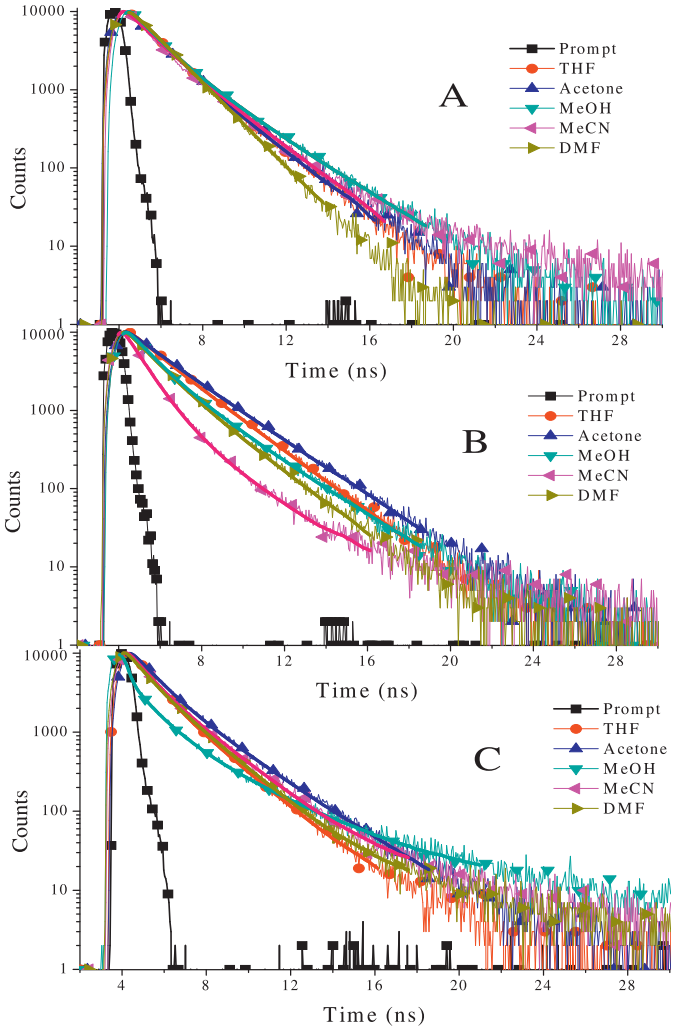

Fig. 5. Typical fluorescence decay curves of compounds BIC (A), BIN (B) and BIR (C) associated with lamp profile in different solvents.

a function of emission wavelength λ_{em} using the single photon counting technique. The full line is the calculated fit assuming an exponential decay convoluted with the instrument response function. Simultaneous curve fitting of the time resolved fluorescence histograms of the compounds as a function of emission wavelength with τ linked over λ_{em}, revealed that the decays are biexponential. The results of lifetime measurements of the compounds are listed in Table 7. All the compounds have two lifetimes; among them the lifetime of major components (52–84%) are long lived one which ranges from 1.16 to 4.05 ns for BIC, 2.33 to 2.95 ns for BIN and 1.97 to 3.35 ns for BIR, and the lifetime of minor component (16–48%) are short lived one which ranges from 1.12 to 1.49 ns for BIC, 0.90 to 1.32 ns for BIN and 0.79 to 1.07 ns for BIR. From Table 7, the short lived lifetime can be assigned to LE transition and the long lived lifetime can be assigned to ICT transition.

Using the experimental fluorescence quantum yield (Φ_f) and averaged lifetime ($\langle\tau\rangle$), the rate constants of radiative (k_r) and nonradiative (k_{nr}) decay were calculated according to Eqs. (6) and (7).

$$k_r = \frac{\Phi_f}{\tau} \tag{6}$$

$$k_{nr} = \frac{1 - \Phi_f}{\tau} \tag{7}$$

From Table 7, BIC has higher Φ_f values results almost equal radiative (k_r) and nonradiative (k_{nr}) constants. But, BIN has very low Φ_f values results very high nonradiative rate constant than the radiative rate constant. This can be ascribed to the presence of NO_2 group which enhances the inter system crossing [61] and internal conversion [62] to the ground state. BIR also exhibits low Φ_f values which can be attributed to the increased nonradiative decay and solvent–solute interactions.

4. Transient absorption

Having characterized in detail the photophysical properties of the compounds in singlet excited state, we performed laser flash photolysis from nano- to the millisecond range in order to obtain information on triplet excited state dynamics. The transient absorption spectra of compounds in DMF solution measured at several delay times from 1 μs to 10 μs after excitation at 355 nm is shown in Fig. 6 (BIR) and SI Figs. 12 and 13 (BIC and BIN, respectively). According to the following Eq. (8), the transient absorption spectrum has contributions from the ground state bleaching (GSB), stimulated emission (SE), excited state absorption (ESA) and triplet state absorption (TSA) [63].

$$\Delta A = \Delta A_{ESA} + \Delta A_{TSA} - \Delta A_{GSB} - \Delta A_{SE} \tag{8}$$

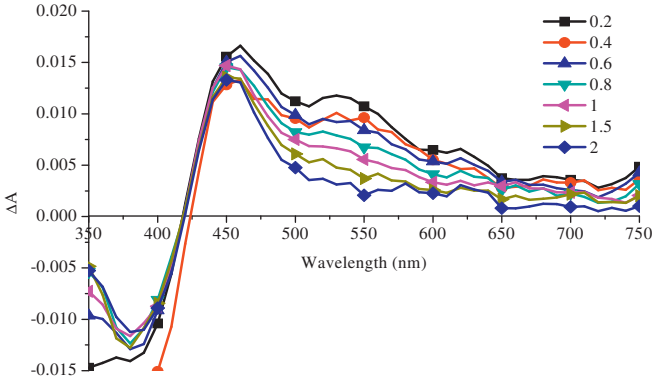

Fig. 6. Transient absorption spectra of BIR in DMF solution (in various μs domains) after excitation at 355 nm.

BIR and BIC exhibited two absorption peaks in the transient spectra among them, and the peak at 450 nm is very stable and long lived over various delay times. However, the peak at 510 nm is less stable and disappeared immediately within few delay times. BIN showed the triplet state absorption peaks at 480 and 530 nm; conversely the long wavelength peak is more stable toward different delay times. Further, the contribution from TSA [64] and GSB has only been observed in the transient spectra and no contribution from stimulated emission has been observed at this time scale [65,66]. The triplet lifetime of the compounds obtained from the kinetic traces at 510 nm for BIC, 480 nm and 540 for BIN are 0.52, 1.29 and 0.99 μs, respectively. Unfortunately, we are unable to calculate the triplet state lifetime of BIR and BIC (at 440 nm) because of long lifetime of the compounds, which are not decayed within the measured time domain.

5. Conclusions

In summary, a series of D-π-A architecture based on 4,5-diphenyl-1H-imidazole moiety as a donor termini connected to biphenyl groups as central spacer with various acceptor groups such as cyanoacetic acid, rhodanine-3-acetic acid and 4-nitrophenyl acetonitrile were synthesized. It was demonstrated that their absorption properties were governed by intramolecular charge separation from the donor to the acceptor fragments. Thermal stability of the compounds analyzed by optical measurements was consistent with the results obtained from thermogravimetric analysis. From Lippert–Mataga treatment, it was proved that the electronically excited state of the fluorophores is substantially more polar than the ground state, which was affirmed by the large solvent-sensitive fluorescence behavior of the compounds. Structure to spectral response of different acceptor groups was also explained by relating the results with BIT which does not have any acceptor groups. Moreover, the origins of the fascinating photophysical properties were also discussed with four-parameter Catalan and Kamlet–Taft approaches. The results of multilinear regression analysis suggested that the emitting state was governed primarily by solvent dipolarity. The structural effect on their optical and electrochemical properties is investigated by DFT, TD-DFT methods and the results give better understanding of electronic structure and absorption spectra of the synthesized molecule. The calculated absorption and emission wavelength of the molecules were relatively in accordance with the experimental results. Contributions of donor and acceptor units toward the electronic transitions were explained with the help of Molecular orbital coefficients analysis. Overall, the studied photophysical properties of imidazole derivatives are of vast significance in the further development of novel molecules in connection with predetermined photophysical properties that will find extensive applications in research fields of current interests.

Supporting information

Absorption and emission spectra of BIN and BIR in various solvents, excitation energy dependant emission spectra in various solvents, transient absorption spectra, TGA, optimized geometry and crystallographic information data.

Acknowledgements

N.N. thank DST-INSPIRE program for the financial assistant as a JRF (IF10495). R.R. and N.N. thank DST, India, for their financial support in the form of a research grant (Ref. No. SR/S1/PC-12/2011, dt. 20/09/2011). G.V. thanks University Grants Commission (UGC), India for the financial support in the form of Science

Meritorious Student Fellowship. P.V. thanks UGC for the award of emeritus fellowship for the Year 2012-13 (Ref. No. F.6-6/2012-13/EMERITUS-2012-13-GEN-1171/(SA-II). We are thankful to Prof. P. Ramamurthy for providing TCSPC and Laser flash photolysis instrumental facilities.

Appendix A. Supplementary data

Supplementary data associated with this article can be found, in the online version, at http://dx.doi.org/10.1016/j.jphotochem.2014.04.008.

References

[1] Q. Li, M. Peng, H. Li, C. Zhong, L. Zhang, X. Cheng, X. Peng, Q. Wang, J. Qin, Z. Li, A. New, Turn-on naphthalenedimide-based chemosensor for mercury ions with high selectivity: successful utilization of the mechanism of twisted intramolecular charge transfer, near-IR fluorescence, and cell images, Org. Lett. 14 (2012) 2094–2097.
[2] K. Hanaoka, Y. Muramatsu, Y. Urano, T. Terai, T. Nagano, Design and synthesis of a highly sensitive off–on fluorescent chemosensor for zinc ions utilizing internal charge transfer, Chem. Eur. J. 16 (2010) 568–572.
[3] L. Xue, C. Liu, H. Jiang, A ratiometric fluorescent sensor with a large Stokes shift for imaging zinc ions in living cells, Chem. Commun. (2009) 1061–1063.
[4] A.C. Arias, J.D. MacKenzie, I. McCulloch, J. Rivnay, A. Salleo, Materials and applications for large area electronics: solution-based approaches, Chem. Rev. 110 (2010) 3–24.
[5] A. Hagfeldt, G. Boschloo, L. Sun, L. Kloo, H. Pettersson, Dye-sensitized solar cells, Chem. Rev. 110 (2010) 6595–6663.
[6] H. Tian, X. Yang, R. Chen, R. Zhang, A. Hagfeldt, L. Sun, Effect of different dye baths and dye-structures on the performance of dye-sensitized solar cells based on triphenylamine dyes, J. Phys. Chem. C 112 (2008) 11023–11033.
[7] D. Srikun, E.W. Miller, D.W. Domaille, C.J. Chang, An ICT-based approach to ratiometric fluorescence imaging of hydrogen peroxide produced in living cells, J. Am. Chem. Soc. 130 (2008) 4596–4597.
[8] S. Soldevila, F. Bosca, Photoreactivity of fluoroquinolones: nature of aryl cations generated in water, Org. Lett. 14 (2012) 3940–3943.
[9] M.A. Ei-Kemary, Photoinduced intramolecular charge transfer of 3-cyano-4-furyl-6-phenyl-2-(9-anthralylidene)-pyridine, J. Photochem. Photobiol. A: Chem. 137 (2000) 9–14.
[10] A.H. Younes, L. Zhu, Tunable dual fluorescence of 3-(2 2′-bipyridyl)-substituted iminocoumarin, ChemPhysChem 13 (2012) 3827–3835.
[11] F.S. Santos, T.M.H. Costa, V. Stefani, P.F.B. Gonçalves, R.R. Descalzo, E.V. Benvenutti, F.S. Rodembusch, Synthesis, characterization, and spectroscopic investigation of benzoxazole conjugated Schiff bases, J. Phys. Chem. A 115 (2011) 13390–13398.
[12] A. Demeter, S.I. Druzhinin, S.A. Kovalenko, T.A. Senyushkina, K.A. Zachariasse, Dual fluorescence and ultrafast intramolecular charge transfer with 6-N,N-dialkylaminopurines. A two-state model, J. Phys. Chem. A 115 (2011) 1521–1537.
[13] N. Mataga, T. Kubota, Molecular Interactions and Electronic Spectra, M. Dekker, New York, 1970.
[14] K.T. Arun, D.T. Jayaram, R.R. Avirah, D. Ramaiah, β-Cyclodextrin as a photosensitizer carrier: effect on photophysical properties and chemical reactivity of squaraine dyes, J. Phys. Chem. B 115 (2011) 7122–7128.
[15] A.B. Nepomnyashchii, M. Bröring, J. Ahrens, A.J. Bard, Synthesis, photophysical, electrochemical, and electrogenerated chemiluminescence studies. Multiple sequential electron transfers in BODIPY monomers, dimers, trimers, and polymer, J. Am. Chem. Soc. 133 (2011) 8633–8645.
[16] C. Vijayakumar, V.K. Praveen, K.K. Kartha, A. Ajayaghosh, Excitation energy migration in oligo(p-phenylenevinylene) based organogels: structure–property relationship and FRET efficiency, Phys. Chem. Chem. Phys. 13 (2011) 4942–4949.
[17] T. Egawa, Y. Koide, K. Hanaoka, T. Komatsu, T. Terai, T. Nagano, Development of a fluorescein analogue, TokyoMagenta, as a novel scaffold for fluorescence probes in red region, Chem. Commun. 47 (2011) 4162–4164.
[18] K.J. Zanotti, G.L. Silva, Y. Creeger, K.L. Robertson, A.S. Waggoner, P.B. Berget, B.A. Armitage, Blue fluorescent dye–protein complexes based on fluorogenic cyanine dyes and single chain antibody fragments, Org. Biomol. Chem. 9 (2011) 1012–1020.
[19] B. Bag, A. Pal, Rhodamine-based probes for metal ion-induced chromo-/fluorogenic dual signaling and their selectivity towards Hg(ii) ion, Org. Biomol. Chem. 9 (2011) 4467–4480.
[20] M. Sarma, T. Chatterjee, S. Ghanta, S.K. Das, D-π-A-A-π-D prototype 2,2′-bipyridine dyads exhibiting large structure and environment-sensitive fluorescence: synthesis, photophysics, and computation, J. Org. Chem. 77 (2011) 432–444.
[21] N. Nagarajan, G. Vanitha, D.A. Ananth, A. Rameshkumar, T. Sivasudha, R. Renganathan, Bioimaging, antibacterial and antifungal properties of imidazole-pyridine fluorophores: synthesis, characterization and solvatochromism, J. Photochem. Photobiol. B: Biol. 127 (2013) 212–222.
[22] C. Congiu, M.T. Cocco, V. Onnis, Design, synthesis, and in vitro antitumor activity of new 1,4-diarylimidazole-2-ones and their 2-thione analogues, Bioorg. Med. Chem. Lett. 18 (2008) 989–993.
[23] L. Nagarapu, A. Satyender, B. Rajashaker, K. Srinivas, P.R. rani, K. Radhika, G. Subhashini, Synthesis and antimicrobial activity of novel C-linked imidazole glycoconjugates, Bioorg. Med. Chem. Lett. 18 (2008) 1167–1171.
[24] R.C. Smith, J.C. Reeves, Antioxidant properties of 2-imidazolones and 2-imidazolthiones, Biochem. Pharmacol. 36 (1987) 1457–1460.
[25] L. Zhou, C. Jia, Z. Wan, Z. Li, J. Bai, L. Zhang, J. Zhang, X. Yao, Triphenylamine-based organic dyes containing benzimidazole derivatives for dye-sensitized solar cells, Dyes Pigm. 95 (2012) 743–750.
[26] D. Kumar, K.R.J. Thomas, C.-P. Lee, K.-C. Ho, Novel pyrenoimidazole-based organic dyes for dye-sensitized solar cells, Org. Lett. 13 (2011) 2622–2625.
[27] S. Park, J.E. Kwon, S.Y. Park, Strategic emission color tuning of highly fluorescent imidazole-based excited-state intramolecular proton transfer molecules, Phys. Chem. Chem. Phys. 14 (2012) 8878–8884.
[28] Y. Yuan, D. Li, X. Zhang, X. Zhao, Y. Liu, J. Zhang, Y. Wang, Phenanthroimidazole-derivative semiconductors as functional layer in high performance OLEDs, New J. Chem. 35 (2011) 1534–1540.
[29] N. Nagarajan, G. Velmurugan, A. Prakash, N. Shakti, M. Katiyar, P. Venuvanalingam, R. Renganathan, Highly emissive luminogens based on imidazo[1 2-a]pyridine for electroluminescent applications, Chem. Asian J. (2013), http://dx.doi.org/10.1002/asia.201301061.
[30] J. Yu, Y. Cui, J. Gao, Z. Wang, G. Qian, Enhanced optical nonlinearity and improved transparency of inorganic–organic hybrid materials containing benzimidazole chromophores, J. Phys. Chem. B 113 (2009) 14877–14883.
[31] M. Velusamy, Y.-C. Hsu, J.T. Lin, C.-W. Chang, C.-P. Hsu, 1-Alkyl-1H-imidazole-based dipolar organic compounds for dye-sensitized solar cells, Chem. Asian J. 5 (2010) 87–96.
[32] C.-H. Chang, Y.-C. Chen, C.-Y. Hsu, H.-H. Chou, J.T. Lin, Squaraine-arylamine sensitizers for highly efficient p-type dye-sensitized solar cells, Org. Lett. 14 (2012) 4726–4729.
[33] J.-Y. Li, C.-Y. Chen, W.-C. Ho, S.-H. Chen, C.-G. Wu, Unsymmetrical squaraines incorporating quinoline for near infrared responsive dye-sensitized solar cells, Org. Lett. 14 (2012) 5420–5423.
[34] Y. Wu, W. Zhu, Organic sensitizers from D-[small pi]-A to D-A-[small pi]-A: effect of the internal electron-withdrawing units on molecular absorption, energy levels and photovoltaic performances, Chem. Soc. Rev. 42 (2013) 2039–2058.
[35] M. Liang, J. Chen, Arylamine organic dyes for dye-sensitized solar cells, Chem. Soc. Rev. 42 (2013) 3453–3488.
[36] M. Singh, R. Kurchania, J.A. Mikroyannidis, S.S. Sharma, G.D. Sharma, An A-D-A small molecule based on the 3,6-dithienylcarbazole electron donor (D) unit and nitrophenyl acrylonitrile electron acceptor (A) units for solution processed organic solar cells, J. Mater. Chem. A 1 (2013) 2297–2306.
[37] J.V. Morris, M.A. Mahaney, J.R. Huber, Fluorescence quantum yield determinations. 9,10-Diphenylanthracene as a reference standard in different solvents, J. Phys. Chem. 80 (1976) 969–974.
[38] N. Dhenadhayalan, C. Selvaraju, P. Ramamurthy, Photoionization and time-dependent Stokes shift of coumarin 307 in soft matter: solvation and radical-ion pair recombination dynamics, J. Phys. Chem. B 115 (2011) 10892–10902.
[39] R. Kumaran, P. Ramamurthy, Denaturation mechanism of BSA by urea derivatives: evidence for hydrogen-bonding mode from fluorescence tools, J. Fluoresc. 21 (2011) 1499–1508.
[40] M.J. Kamlet, J.L.M. Abboud, M.H. Abraham, R.W. Taft, Linear solvation energy relationships. 23. A comprehensive collection of the solvatochromic parameters, pi, alpha, and beta, and some methods for simplifying the generalized solvatochromic equation, J. Org. Chem. 48 (1983) 2877–2887.
[41] J. Catalán, Toward a generalized treatment of the solvent effect based on four empirical scales: dipolarity (SdP, a new scale), polarizability (SP), acidity (SA), and basicity (SB) of the medium, J. Phys. Chem. B 113 (2009) 5951–5960.
[42] A.D. Becke, Density-functional thermochemistry. III. The role of exact exchange, J. Chem. Phys. 98 (1993) 5648–5652.
[43] J.P. Perdew, Density-functional approximation for the correlation energy of the inhomogeneous electron gas, Phys. Rev. B 33 (1986) 8822–8824.
[44] A.D. Becke, Density-functional exchange-energy approximation with correct asymptotic behavior, Phys. Rev. A 38 (1988) 3098–3100.
[45] C. Lee, W. Yang, R.G. Parr, Development of the Colle–Salvetti correlation-energy formula into a functional of the electron density, Phys. Rev. B 37 (1988) 785–789.
[46] J.B. Foresman, M. Head-Gordon, J.A. Pople, M.J. Frisch, Toward a systematic molecular orbital theory for excited states, J. Phys. Chem. 96 (1992) 135–149.
[47] R.E. Stratmann, G.E. Scuseria, M.J. Frisch, An efficient implementation of time-dependent density-functional theory for the calculation of excitation energies of large molecules, J. Chem. Phys. 109 (1998) 8218–8224.
[48] E. Runge, E.K.U. Gross, Density-functional theory for time-dependent systems, Phys. Rev. Lett. 52 (1984) 997–1000.
[49] T. Yanai, D.P. Tew, N.C. Handy, A new hybrid exchange–correlation functional using the Coulomb-attenuating method (CAM-B3LYP), Chem. Phys. Lett. 393 (2004) 51–57.
[50] S. Miertuš, E. Scrocco, J. Tomasi, Electrostatic interaction of a solute with a continuum. A direct utilization of AB initio molecular potentials for the prevision of solvent effects, Chem. Phys. 55 (1981) 117–129.
[51] M.J. Frisch, G.W. Trucks, H.B. Schlegel, G.E. Scuseria, M.A. Robb, J.R. Cheeseman, G. Scalmani, V. Barone, B. Mennucci, G.A. Petersson, H. Nakatsuji, M. Caricato,

X. Li, H.P. Hratchian, A.F. Izmaylov, J. Bloino, G. Zheng, J.L. Sonnenberg, M. Hada, M. Ehara, K. Toyota, R. Fukuda, J. Hasegawa, M. Ishida, T. Nakajima, Y. Honda, O. Kitao, H. Nakai, T. Vreven, J.A. Montgomery, J.E. Peralta, F. Ogliaro, M. Bearpark, J.J. Heyd, E. Brothers, K.N. Kudin, V.N. Staroverov, R. Kobayashi, J. Normand, K. Raghavachari, A. Rendell, J.C. Burant, S.S. Iyengar, J. Tomasi, M. Cossi, N. Rega, J.M. Millam, M. Klene, J.E. Knox, J.B. Cross, V. Bakken, C. Adamo, J. Jaramillo, R. Gomperts, R.E. Stratmann, O. Yazyev, A.J. Austin, R. Cammi, C. Pomelli, J.W. Ochterski, R.L. Martin, K. Morokuma, V.G. Zakrzewski, G.A. Voth, P. Salvador, J.J. Dannenberg, S. Dapprich, A.D. Daniels, Farkas, J.B. Foresman, J.V. Ortiz, J. Cioslowski, D.J. Fox, Gaussian 09, Revision B.01, Gaussian, Inc., Wallingford, CT, 2009.

[52] Y. Zhang, S.-L. Lai, Q.-X. Tong, M.-F. Lo, T.-W. Ng, M.-Y. Chan, Z.-C. Wen, J. He, K.-S. Jeff, X.-L. Tang, W.-M. Liu, C.-C. Ko, P.-F. Wang, C.-S. Lee, High efficiency nondoped deep-blue organic light emitting devices based on imidazole-π-triphenylamine derivatives, Chem. Mater. 24 (2011) 61–70.

[53] D. Kumar, K.R.J. Thomas, C.-C. Lin, J.-H. Jou, Pyrenoimidazole-based deep-blue-emitting materials: optical, electrochemical, and electroluminescent characteristics, Chem. Asian J. 8 (2013) 2111–2124.

[54] M. Wächtler, M. Maiuri, D. Brida, J. Popp, S. Rau, G. Cerullo, B. Dietzek, Utilizing ancillary ligands to optimize the photophysical properties of 4H-imidazole ruthenium dyes, ChemPhysChem 14 (2013) 2973–2983.

[55] B. Ramachandram, A. Samanta, Modulation of metal-fluorophore communication to develop structurally simple fluorescent sensors for transition metal ions, Chem. Commun. (1997) 1037–1038.

[56] A.L. Tenderholt, QMForge, Version 2.1, Standford University, Standford, CA, USA, 2007.

[57] D. Kumar, K.R.J. Thomas, Optical properties of pyrene and anthracene containing imidazoles: experimental and theoretical investigations, J. Photochem. Photobiol. A: Chem. 218 (2011) 162–173.

[58] S.S. Bag, R. Kundu, Installation/modulation of the emission response via click reaction, J. Org. Chem. 76 (2011) 3348–3356.

[59] K. Guzow, M. Czerwinska, A. Ceszlak, M. Kozarzewska, M. Szabelski, C. Czaplewski, A. Lukaszewicz, A.A. Kubicki, W. Wiczk, Photophysical properties of 3-[2-(N-phenylcarbazolyl)benzoxazol-5-yl]alanine derivatives – experimental and theoretical studies, Photochem. Photobiol. Sci. 12 (2013) 284–297.

[60] E. Krystkowiak, K. Dobek, A. Maciejewski, An intermolecular hydrogen-bonding effect on spectral and photophysical properties of 6-aminocoumarin in protic solvents, Photochem. Photobiol. Sci. 12 (2013) 446–455.

[61] C.E. Crespo-Hernández, G. Burdzinski, R. Arce, Environmental photochemistry of nitro-PAHs: direct observation of ultrafast intersystem crossing in 1-nitropyrene, J. Phys. Chem. A 112 (2008) 6313–6319.

[62] V.M. Farztdinov, R. Schanz, S.A. Kovalenko, N.P. Ernsting, Relaxation of optically excited p-nitroaniline: semiempirical quantum-chemical calculations compared to femtosecond experimental results, J. Phys. Chem. A 104 (2000) 11486–11496.

[63] H. Imahori, S. Kang, H. Hayashi, M. Haruta, H. Kurata, S. Isoda, S.E. Canton, Y. Infahsaeng, A. Kathiravan, T.R. Pascher, P. Chábera, A.P. Yartsev, V. Sundstrom, Photoinduced charge carrier dynamics of Zn–Porphyrin–TiO_2 electrodes: the key role of charge recombination for solar cell performance, J. Phys. Chem. A 115 (2010) 3679–3690.

[64] A.I. Ciuciu, K. Skonieczny, D. Koszelewski, D.T. Gryko, L. Flamigni, Dynamics of intramolecular excited state proton transfer in emission tunable, highly luminescent imidazole derivatives, J. Phys. Chem. C 117 (2013) 791–803.

[65] L. Zedler, S. Kupfer, I.R. de Moraes, M. Wächtler, R. Beckert, M. Schmitt, J. Popp, S. Rau, B. Dietzek, Trapped in imidazole: how to accumulate multiple photoelectrons on a black-absorbing ruthenium complex, Chem. Eur. J. 20 (2014) 3793–3799.

[66] M. Wächtler, S. Kupfer, J. Guthmuller, S. Rau, L. González, B. Dietzek, Structural control of photoinduced dynamics in 4H-imidazole-ruthenium dyes, J. Phys. Chem. C 116 (2012) 25664–25676.